Bulletin of the Seismological Society of America, Vol. 83, No. 2, pp. 509–528, April 1993

TOMOGRAPHY WITHOUT RAYS

By Charles J. Ammon and John E. Vidale

Abstract

We present two new techniques for the inversion of first-arrival times to estimate velocity structure. These travel-time inversion techniques are unique in that they do not require the calculation of ray paths. First-arrival times are calculated using a finite-difference scheme that iteratively solves the eikonal equations for the position of the wavefront. The first inversion technique is a direct extension of linearized waveform inversion schemes. The nonlinear relationship between the observed first-arrival times and the model slowness is linearized using a Taylor series expansion and a solution is found by iteration. For a series of two-dimensional numerical tests, with and without random noise, this travel-time inversion procedure accurately reconstructed the synthetic test models. This iterative inversion procedure converges quite rapidly and remains stable with further iteration. The second inversion technique is an application of simulated annealing to travel-time topography. The annealing algorithm is a randomized search through model space that can be shown to converge to a global minimum in well-posed problems. Our tests of simulated annealing travel-time topography indicate that, in the presence of less than ideal ray coverage, significant artifacts may be introduced into the solution. The linearized inversion scheme outperforms the nonlinear simulated annealing approach and is our choice for travel-time inversion problems. Both techniques are applicable to a variety of seismic problems including earthquake travel-time tomography, reflection, refraction/wide-angle reflection, borehole, and surface-wave phase-velocity tomography.

Introduction

Seismic methods are perhaps our most valuable tool in the study of *in situ* subsurface geology. From among the many seismic techniques, a particularly robust method for imaging velocity variations is the inversion of first-arrival times. First-arrival times are most reliably picked from the seismic records since they are not contaminated by signal-generated noise that can complicate the identification and picking of later-arriving phases. Whether the data are from an active (reflection or refraction experiment) or passive (earthquake) source experiments, the basic inversion techniques are fundamentally identical. Crisscrossing wave paths are used to separate the integrated effects of slowness on travel time and construct an image of the underlying velocity structure.

Tomographic techniques have been applied to travel-time or phase observations for most seismic wave types. In a typical tomographic application, the inverse problem is linearized and the ray paths through a simple (homogeneous, layered, spherically symmetric, etc.) reference model are calculated and the anomalies in travel time are projected back along these paths. Fermat's principle justifies this approximation in mildly heterogeneous media, but this simplification is often motivated by the fact that, in heterogeneous media, two-point raytracing is computationally expensive and difficult. Rays connecting two points are often difficult to find and deciding whether a given ray is the least-time path through the model is also difficult. The solution to the eikonal

equation we employ (Vidale 1988, 1991) quickly calculates the minimum arrival time from a source location to each point in the model. In the presence of extreme velocity gradients, solutions of the eikonal equations are not always good approximate solutions of the wave equation, and Vidale's (1988, 1991) original scheme may be inaccurate. Vidale (1993) addresses the problems with large velocity contrasts and outlines a recursive algorithm for the computation of first arrival times in two-dimensional, strongly heterogeneous media. This recursive algorithm requires more computations, but in our experience the increase in computer time is modest. Both of the inversion techniques described below are independent of the method used to calculate the travel times. Our choice of the finite-difference travel-time calculation scheme was based on computational efficiency. This choice contributes the originality of our approach, because it does not require a specific knowledge of ray paths.

We begin with a discussion of an approach to travel-time inversion using a linearized least-squares technique. This approach is commonly applied in waveform inversion problems, but it is not the usual approach for tomographic problems. The travel-time inversion proceeds by expanding the nonlinear relationship between the slowness model and the travel times in a Taylor series and iterating to a solution. Smoothness constraints are placed on the solutions by minimizing a measure of model roughness. We illustrate the technique using a series of synthetic test inversions without and with noise added to the travel times.

We then compare the results of a linearized inversion with the results of a second scheme for modeling travel times, a simulated annealing inversion. Simulated annealing is a nonlinear, Monte-Carlo–based optimization scheme in which a randomized search for solutions is conducted. The algorithm is computationally intensive in that many forward calculations are required during the search. For well-posed problems (in the sense that all the model parameters are well constrained by the data), a simulated annealing search will converge to the global minimum. This is not always the case in geophysical problems where features may be added to a model without affecting the observations. In the tomographic problem such features are known as ghosts (Berryman, 1990); in linear inverse theory, these ghosts are vectors in the null space of the inverse operator.

We conclude by presenting a linearized inversion of Rayleigh-wave phase velocities to estimate the phase-velocity distribution beneath the western United States. We make no interpretation of the result and only use the inversion as an illustration of the linearized inversion scheme's performance on realistically distributed, noisy earthquake observations. We also discuss a technique for rapidly identifying areas of the model that are sensitive to specific travel-time observations. This information can lead to significant time savings for the linearized inversions that require many travel-time calculations to estimate partial derivatives of the travel times with respect to model slowness values.

Although we do not discuss resolution and uniqueness, these topics are critical for applications of any inversion technique. However, the primary goal in this paper is to illustrate two new tomographic techniques that do not require the calculation of ray paths, not to analyze tomographic resolution and uniqueness. For discussions of these issues, we refer the reader to the discussions found in the literature (Nolet, 1987).

The Linearized Least-Squares Inversion of Travel Times

Several expositions on seismic travel-time tomography are available in the literature. We will not discuss the fundamental theory behind the technique, but refer the reader to published reviews (for example, Nolet, 1987; Berryman, 1989b, 1990). We consider a discrete travel-time inversion problem where absolute travel times are available. The slowness model consists of discrete, constant slowness cells and the data set consists of a finite number of travel-time observations. The relationship between the travel times $\boldsymbol{t}$ and the slowness $\boldsymbol{s}$ can be expressed by the matrix equation

$$\mathbf{t} = \mathbf{L}\mathbf{s}. \tag{1}$$

$\boldsymbol{L}$ is a matrix containing the lengths of the ray paths through each individual slowness cell. This relationship is nonlinear since the ray paths that define the matrix $\boldsymbol{L}$ depend on the slowness vector $\boldsymbol{s}$. Solution of (1) is possible by beginning with an initial model and iterating to the correct slownesses and ray paths, an approach most often taken in nonlinear travel-time inversion problems (e.g., Berryman, 1989b).

An alternative approach is to deal not with rays but with the functional description of the travel-time equation

$$\mathbf{t} = F[\mathbf{s}]. \tag{2}$$

The nonlinear function F represents the calculation of travel times through the particular slowness model, $\mathbf{s}$. We can expand $F[\mathbf{s}]$ about an initial model, $\mathbf{s}_0$, resulting in

$$\mathbf{t} = F[\mathbf{s}_0] + \mathbf{D}\delta\mathbf{s} + \mathbf{O}\|\delta\mathbf{s}^2\|. \tag{3}$$

The matrix $\mathbf{D}$ contains the partial derivatives of the travel times with respect to slowness, $\delta\mathbf{s}$ is a slowness correction vector. Neglecting the higher order terms in $\delta\mathbf{s}$ and rearranging the equation, we find that

$$\mathbf{t} - F[\mathbf{s}_0] \approx \mathbf{D}\delta\mathbf{s}. \tag{4}$$

The left-hand side of equation (4) is a travel-time residual vector, and the right-hand side is a simple matrix multiplication. Bregmen *et al.* (1989) derived a similar expression for the inversion for velocity using the partial derivatives of travel time with respect to velocity. Equation (4) can be solved using standard least-squares approaches (Jackson, 1972; Wiggins, 1972). The final estimate is approached by iterating (4) and updating the current estimate with the correction vector $\delta\boldsymbol{s}$. Smoothness or other constraints can be applied to the slowness correction vector during the solution of (4) (see, for example, Lees and Crosson, 1989). A more direct approach is to apply constraints on the model smoothness. Following Shaw and Orcutt (1985), we add $\mathbf{D}\mathbf{s}_0$ to both sides of (4), producing

$$\mathbf{t} - F[\mathbf{s}_0] + \mathbf{D}\mathbf{s}_0 \approx \mathbf{D}\mathbf{s}. \tag{5}$$

Equation (5) is identical in form to equation (4) but allows easy implementation of smoothness or other constraints on the resulting model $\mathbf{s}$. We use equation (5) in an iterative fashion to converge to a slowness vector that minimizes the length of the travel-time residual vector, $\mathbf{r}$.

To implement the smoothness constraints, we modify (5) to include a set of equations that require the Laplacian difference of the model to vanish. We weight the smoothness constraint equations relative to the travel-time equations to solve for a smooth model that is consistent with the travel-time observations. The iterative equations become

$$\begin{bmatrix} \mathbf{r}_{i-1} \\ 0 \end{bmatrix} + \begin{bmatrix} \mathbf{D}\mathbf{s}_{i-1} \\ 0 \end{bmatrix} = \begin{bmatrix} \mathbf{D} \\ \lambda\boldsymbol{\Delta} \end{bmatrix} \mathbf{s}_i. \tag{6}$$

$\boldsymbol{s}_i$ is the solution of the ith iteration of the problem, $\mathbf{s}_{i-1}$ is the solution from the previous iteration, and $\mathbf{D}$ is calculated using $\mathbf{s}_{i-1}$. The weighting factor λ controls the trade-off between fitting the travel times and smoothing the model. The submatrix $\boldsymbol{\Delta}$ constructs the Laplacian of the slowness image, and so we have added a system of equations to the original travel-time inversion problem

$$4S_{x,z} - S_{x-dx,z} - S_{x+dx,z} - S_{x,z-dz} - S_{x,z+dz} = 0. \tag{7}$$

For cells along the edges of the image the cell outside the image in (7) is replaced by the average of the three cells adjacent to the edge cell. Similarly, at the corners the missing cells are replaced by the average of the two cells adjacent to the corner cell. Weighting the edge and corner cells of the model equally with the interior cells is important for a successful implementation of the smoothness constraint. The cells in the interior of the image appear in five constraining equations. Cells on the edge appear in four equations and the corner cells appear in three constraints. To produce equal weighting, simply multiply the edge constraint equations by 5/4 and the corner constraints by 5/3. The constraint on the Laplacian is not a lowpass filter in the classical sense; not all sharp contrasts in the model are necessarily smoothed. The total amount of slowness fluctuation, not individual slowness constrasts, is limited.

Synthetic Tests

We performed several synthetic tests using the linearized travel-time inversion technique described above. The tests are designed to examine convergence and stability properties. Each test model consisted of a rectangular image twice as tall as it is wide. In each example, 128 (8 by 16) velocity values are sought, and, unless otherwise noted, 320 travel-time observations are inverted. The finite-difference travel-time calculations are performed for a model defined by velocity nodes. To provide sufficient accuracy in the travel time calculations, we magnify the 8 by 16 velocity models to a dimension of 32 by 64 nodes before calculating the travel times. Magnification produces a model in which groups of adjacent velocity nodes have equal velocity. For example, the first four nodes in the first four rows in the upper left of our synthetic models will have the same velocity. We will refer to groups of constant velocity nodes as cells. Thus, our models contain 32 by 64 nodes, but only 8 by 16 cells. The appropriate magnification factor will depend on the accuracy necessary in the travel times. A simple method to estimate the appropriate magnification is to calculate travel times through a model with increasing levels of magnification. When little change in travel time is observed for successively larger magnifications, the approapriate magnification factor has been reached. For two-dimensional models, the travel-

time computation requirements for a larger magnification increase as the square of the magnification factor linearly in each spatial dimension.

To calculate the partial derivatives for the matrix **D** of equation (6), we perturb each velocity cell individually (with a perturbation amplitude of +0.5% slowness) and use a one-sided finite-difference approximation to the derivative. Thus to construct the partial derivative matrix, we require one plus the number of cells forward calculations. For 128 cells and 320 observations, 41,280 cell arrival times are calculated for each iteration (129 forward calculations). The smoothness constraints add an additional 128 equations to the inversion. We solve the matrix equation by inverting the 448 by 128 matrix using singular value decomposition. The smoothness constraints provide stability for the inversions described below, and no singular value truncation is necessary. This may not always be the case, some smooth components of the model may be poorly constrained and additional constrants or damping may be necessary.

Figure 1 shows the first test model, which is similar to a model constructed by Berryman (1989a) to test a ray-based inversion scheme. The model consists of a constant velocity medium with both 20% low- and 20% high-velocity anomalies. The slowness anomalies associated with these velocity anomalies are different (25% for the slow anomaly and 17% for the fast anomaly). The accurate imaging of such large velocity anomalies requires an approach that includes the effects of wave refraction. Figure 1 also contains the source and receiver locations used in all the synthetic tests. Each source located along the top of the model transmits energy to each receiver placed along the bottom of the image, and each source along the left of the model transmits energy to each receiver along the right side of the model.

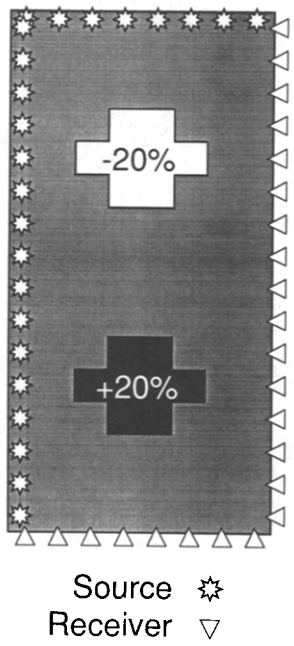

FIG. 1. "Cross Model" and the source-receiver distribution for the first synthetic test. The perturbations are in velocity. The top sources radiate to receivers along the bottom of the model, while the sources along the left side of the image radiate energy to the receivers along the right side of the model. The perturbation positions and shapes are patterned after Berryman (1989a).

The travel-time residuals between the heterogeneous model shown in Figure 1 and a model with a velocity equal to the background velocity of the heterogeneous model range between 4% and 10%. Figure 2 presents the travel-time residual curves for two sources. The receiver order is from left to right for the upper diagram and from top to bottom for the lower diagram. In a scaled problem, the amplitude of the residuals depends on the problem scale factor, the numbers shown correspond to a unit background velocity and a physical cell dimension of 4 units. To put these residuals in perspective, if we assume a background velocity of 1 km/sec, the minimum and maximum travel times through this model are about 30 and 70 sec, respectively. We mention that the source-receiver distribution is nearly, but not exactly, symmetric with respect to the model bounds and the position of the heterogeneities.

The first step in the inversion of the travel times is to estimate an appropriate value of the smoothness control parameter λ. The magnitude of λ necessary for a specified amount of smoothing depends on the magnitude of the partial derivatives corresponding to the problem. The simplest technique for estimating λ is to perform at least one iteration of the inversion for a range of λ values and choose the λ value that produces best trade-off between travel-time fit and model smoothness. In Figure 3 we present the trade-off curve between the L_2 Error and the model roughness. The L_2 Error is explicitly

$$L_2 = \frac{1}{N} \sum_{i=1}^{N} \left(t_i^{obs} - t_i^{calc} \right)^2, \tag{8}$$

where N is the number of observed times, t_i^{obs} is the observed travel time, and

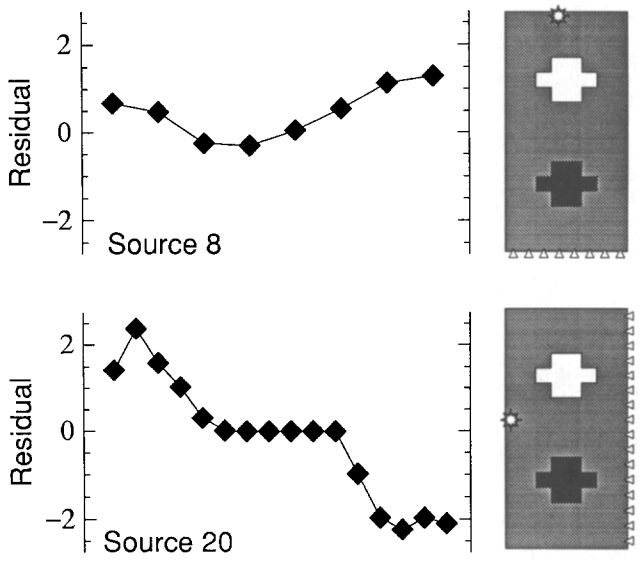

FIG. 2. Example of the traveltime residuals between the "Cross Model" and a constant velocity model. Corresponding source receiver geometry is shown to the right. Receiver ordering is from left-to-right (*upper*) and from top-to-bottom (*lower*).

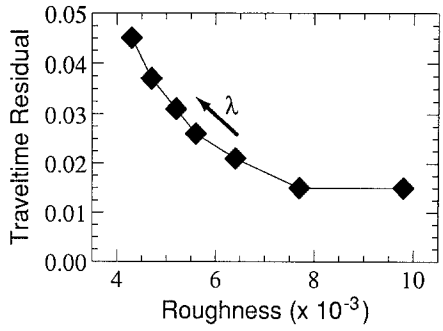

FIG. 3. Travel-time residual versus model roughness trade-off curve for seven inversions of the "Cross Model" travel times. The smoothness control parameter 1 varies from 1 to 7 in the direction indicated by the arrow. The travel-time residual for a constant velocity model is 1.69.

t_i^{calc} is the calculated travel time. The roughness is defined as

$$R = \frac{1}{M} \sum_{c=1}^{M} (\nabla_c^2 s_c)^2. \tag{9}$$

The discrete Laplacian operator is defined in equation (7), M is the number of slowness cells, and s_c is the slowness. Each point represents the result of a five-iteration inversion beginning with a constant velocity initial model (constant velocity equal to the background velocity of the "target" model). The corresponding λ values vary from 1 to 7 in steps of 1, from right to left. For reference, the L_2 travel-time residual for the constant velocity model is 1.69. Figure 4 contains four of the solutions. The fit for all λ is acceptable, and choosing the preferred value is somewhat subjective. From Figure 3, the solution for $\lambda = 2$ provides the lowest error and a smoother model than $\lambda = 1$. For this reason and because of other empirical tests, we have chosen the value of $\lambda = 2$ for the remainder of the synthetic tests.

All the reconstructions are acceptable. The inversions image the high-velocity anomaly well, although minor blurring of the feature occurs. As expected, imaging the low-velocity heterogeneity is more difficult (a larger slowness anomaly) and the reconstructions underestimate the overall size and amplitude of this perturbation. However, each image has significantly low velocities in the region of the true low velocities so the feature would certainly not be missed. The maximum velocity estimated by the inversions is within 1% of the target high velocity and the lowest velocity estimated is within 4% of the target low velocity.

Figure 5 presents the results of an inversion in the presence of various levels of uniformly distributed random travel-time errors. The number at the top of each image identifies the maximum amplitude of the added error. The effects of the errors only become significant when the error amplitude equals approximately half the amplitude of the inverted travel-time residuals (Fig. 2), which is about 2% of a typical travel time. The smoothness control parameter was equal to 2 for each of the inversions in Figure 5. Figure 6 presents the results of an inversion with ± 1.0 noise with increasing λ. Table 1 contains the corresponding errors and roughnesses.

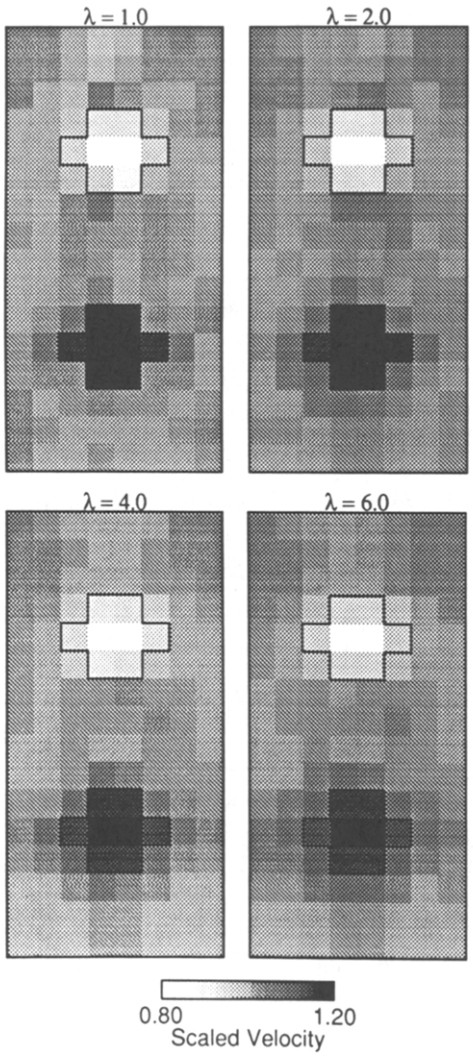

FIG. 4. Reconstructions of the "Cross Model" for a suite of smoothness control parameter values. The smoothness control parameter value is indicated above each image.

There is not a very large dependence of travel time error on λ. The rougher models fit slightly better, but clearly, in the presence of noise, smoothness should be an important criterion in the selection of a preferred model. The tests show that, when noise may be a problem, increasing the weighting for a smooth model is more desirable than fitting all the details in the noisy travel times.

To demonstrate the stability and convergence properties of the inversion scheme, we generated "synthetic data" for more complicated, but also smoother velocity structures. Figure 7 contains the inversion results for three such velocity structures. The target velocity structures are shown above the reconstructions. The model on the left will be referred to as smooth model 1, the center model as smooth model 2, and the model on the right as smooth model 3. The velocity structures were generated by beginning with a constant velocity background and adding a perturbation function to the image. The perturbation

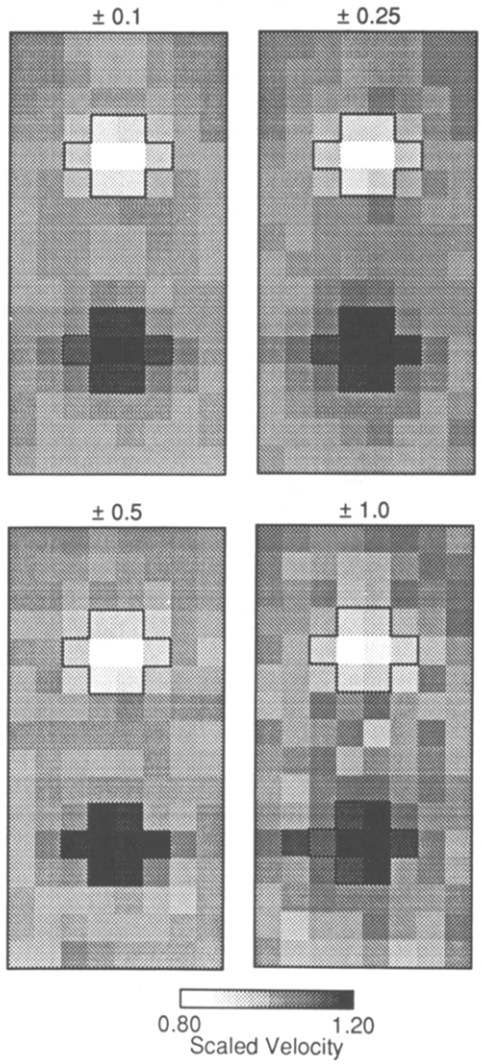

FIG. 5. Reconstructions of the "Cross Model" with varying levels of uniformly distributed random noise added to the travel-time residuals. The maximum absolute amplitude of the random noise is shown above each image. The smoothness control parameter for each reconstruction was 2.0.

functions are constructed by generating a spatially random image and lowpass filtering in the wavenumber domain. The resulting perturbation functions are then scaled to a maximum velocity fluctuation and added to the constant velocity models. The target or "solution" models contain a four-fold finer spatial sampling than the reconstructions and are thus 32 by 64 in dimension. The source-receiver distribution is identical to that used in the earlier test. Each inversion began with the same constant velocity initial model and the results are presented after five iterations. The smoothness control parameter, λ, was equal to 2.0 for each of the inversions, and the synthetic travel times are noise-free. Inspection of Figure 7 reveals that the inversion scheme reconstructs even the minor details of each image quite well and is free of artifacts. The ratios of the final L_2 error to the constant valocity model error for the three inversions are 3×10^{-4}, 3×10^{-4}, and 1×10^{-4}, respectively. The inversions

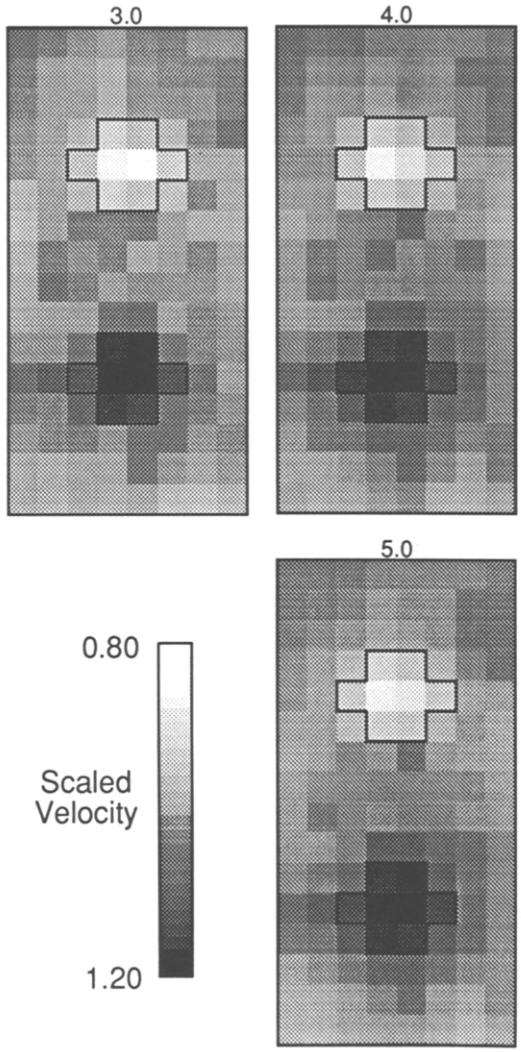

FIG. 6. Inversion results for the "Cross Model" in the presence of traveltime noise for a range of smoothness control parameters. The maximum amplitude of the random time noise is ± 1.0. The smoothness control parameter is shown above each image.

TABLE 1

RESULTS FROM INVERSIONS WITH UNIFORMLY DISTRIBUTED RANDOM NOISE TEST WITH $-1.0 \leqq \Delta T \leqq 1.0$

λ	L_2 Error	Roughness ($\times 10^{-3}$)
2	0.266	11.3
3	0.264	8.2
4	0.280	6.2
5	0.288	5.2

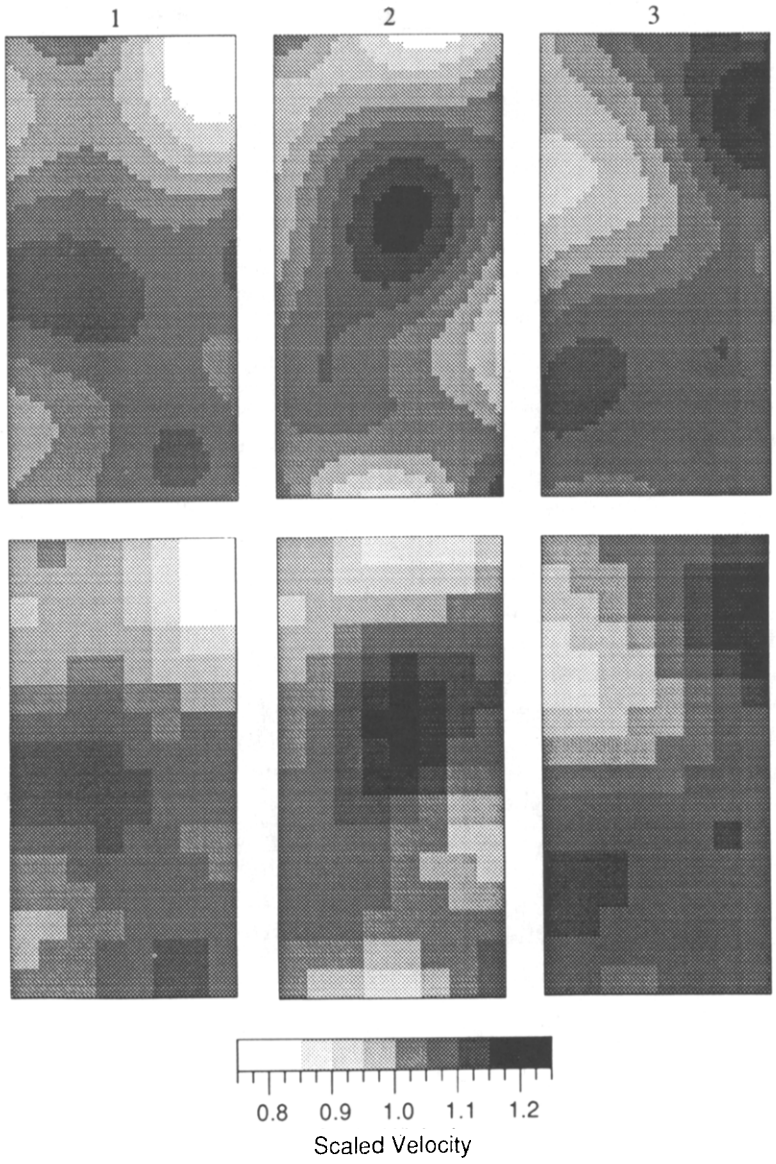

FIG. 7. Inversion results for three smooth models. (*Top*) Target models for the inversion tests. (*Bottom*) Inversion results (after five iterations). Smoothness control parameter for the inversions was 2.0.

converge quickly and are stable as is illustrated in Figure 8, a plot of the travel-time residual versus iteration for the smooth model 1.

SIMULATED ANNEALING INVERSIONS

We also investigated the application of simulated annealing to the travel-time inversion problem. Simulated annealing is a randomized search procedure designed by analogy with the cooling of a melt into a crystal (Kirkpatrick *et al.*, 1983; Aarts and Korst, 1989). Rothman (1985) introduced the simulate annealing to geophysics and along with other researchers has investigated optimiza-

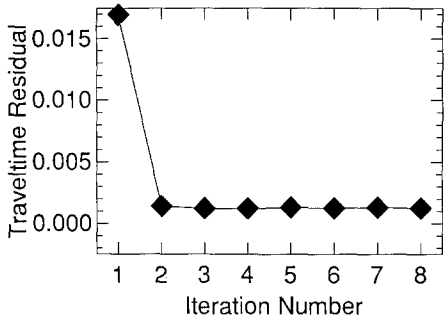

FIG. 8. Travel-time residual as a function of iteration for the smooth velocity model 1. Note the quick convergence and the stability of the solution upon successive interactions.

tion techniques constructed by analogy with optimizing systems found in nature (Landa *et al.*, 1989; Frazer, 1990). For a detailed discussion of simulated annealing, see Rothman (1985, 1986) or Tarantola (1987). We present a brief review similar to the discussion in Press *et al.* (1988).

For a simulated annealing inversion, the travel-time error is analogous to the energy of a cooling melt. We search for the slownesses model that produces a minimum travel-time error; a melt seeks an atomic arrangement that produces a minimum energy configuration. A melt, if allowed to cool slowly, will find a global energy minimum. Our assumption is that, if our search mimics the cooling of a melt, our final slowness configuration will also be a global minimum. Thus we construct the rules for our search using the physical laws governing the cooling melt.

At any particular instant, the melt will make changes in its atomic configuration and an associated change in energy takes place. For a melt at thermodynamic equilibrium, the energy is distributed with the Boltzmann probability function

$$P(E) \alpha \exp\left(\frac{-E}{kT}\right). \tag{10}$$

$P(E)$ is the probability distribution of the melt's energy, E is the energy, k is Boltzmann's constant, and T is temperature. Even at very low temperatures, there is a small possibility that the melt will be at a high state of energy. Occasional transitions from a lower to higher energy state enables the melt to avoid local energy minima. The probability of an "up-hill" transition depends on the crystal temperature. At high temperatures, the melt is hot and many transitions to higher states of energy occur. As the crystal cools the up-hill transitions are accepted less frequency. Metropolis *et al.* (1953) modeled thermodynamic systems using these principles and developed the scheme where the transition from one configuration to another obeyed a Boltzmann probability distribution for the change in energy

$$P(E_A \rightarrow E_B) \alpha \exp\left(\frac{-\Delta E}{kT}\right). \tag{11}$$

ΔE is the change in energy between configurations A and B. The Metropolis algorithm proceeds as follows: A random change is made to the current configuration and the energy of this perturbed model is evaluated. If the energy of the perturbed model is less than the initial model, the proposed transition is accepted. If the model perturbation results in a higher energy state, the transition is accepted with the probability (11).

To mimic the cooling melt in a randomized search for an optimal slowness model, we construct model perturbations and test them to see if they improve or degrade the fit to the observed travel times. If the travel-time residual decreases, we unconditionally accept the perturbation and our model completes a transition. If the perturbation causes the travel-time misfit to increase, we still allow the possibility for the acceptance of this model. Specifically, we accept an increase in error if the right-hand side of (11) (ΔE represents the change in travel-time residual) is greater than a selection from a uniform distribution of random numbers.

We have ignored a very important parameter in (11), the product kT. No physical analog exists for this number in the travel-time optimization problem, although Tarantola (1987) has compared it to the data variance. This quantity is related to the rate at which the melt cools and thus will be related to the rate at which the search for a travel-time minimum converges to a minimum. We combine kT into a single parameter called the control parameter. We specify a cooling schedule for the search using the control parameter. In problems involving local minima, the results of our search can depend greatly on this choice. Two desirable properties of the temperature function are the following: (1) early in the search, it produces an acceptance probability near unity; (2) it decreases slowly enough to allow an escape from local minima during the search. Condition (1) reduces the dependence of the search on the initial model. Meeting the second requirement is more difficult since a practical consideration is that convergence to a model occurs within a reasonable amount of computing time. A simple choice for the control parameter, C, is (Aarts and Korst, 1989)

$$C_{k+1} = \gamma C_k. \tag{12}$$

γ is a number very near, but less than 1, and k is the number of the current transition in the search.

We construct our velocity perturbations with the same procedure used to generate the smooth velocity models tested above. First, we generate a random perturbation velocity field and then lowpass filter the perturbation with a Gaussian filter. The width of the lowpass filter is allowed to vary randomly during the search, but the maximum absolute amplitude of any perturbation image is fixed to 1% of the background velocity model.

Figure 9 contains the results of three different simulated annealing inversions of the first arrival times calculated through the velocity model shown in Figure 1. The value of γ for these inversions was 0.998318, and the initial value of the control parameter was 0.25. Each search contained a total of 2000 proposed transitions. The sharp features of the Cross Model are not reconstructed since the perturbations are always smooth functions with a Gaussian correlation. The travel-time errors associated with each model are 0.16, 0.18, 0.19, from left to right, respectively. All three reconstructions are reasonable, the low- and high-velocity regions are both imaged. Additional artifacts of the

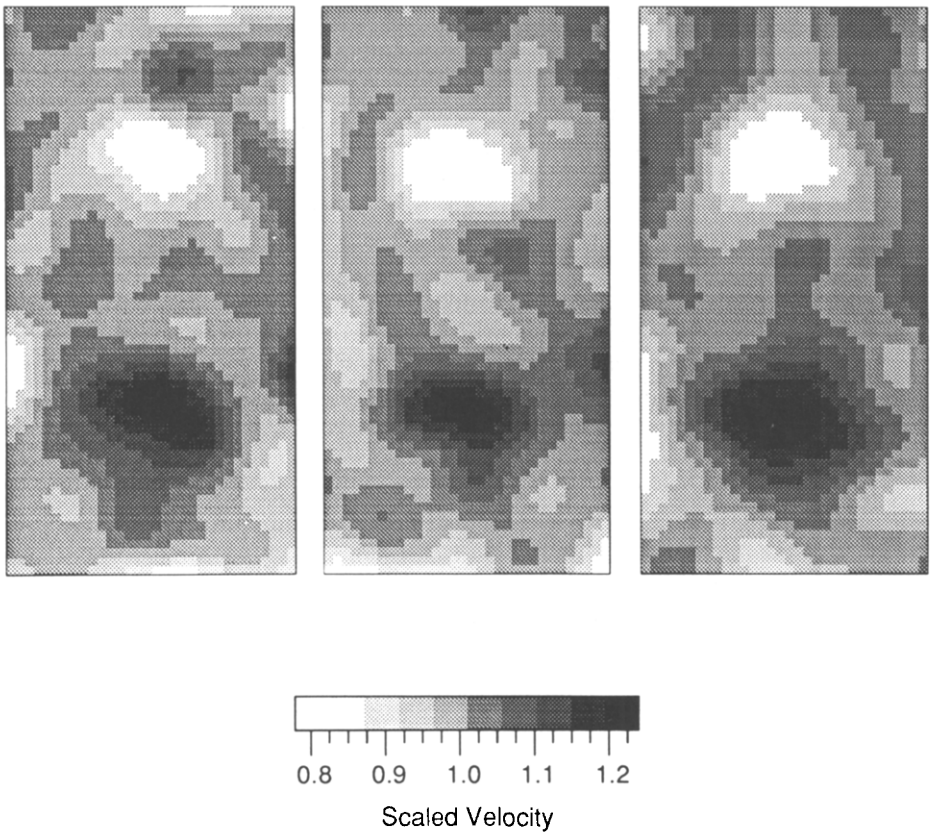

FIG. 9. Simulated annealing inversion results for three different searches. Each search consisted of 2000 perturbations starting from a constant background initial model.

perturbation scheme are also present. Note that the spurious features in each reconstruction are for the most part uncorrelated between the models. This suggests that averaging the three models may reduce unconstrained aspects of each solution and produce a model that fits the travel times better. The average of the three models in Figure 9 is presented in Figure 10 along with the result from the linearized inversion and a result from a straight ray tomography solution of the same tomographic problem. The travel-time residual for the linearized inversion result is 0.02, and the travel-time residual for the straight ray backprojection is 0.39.

Overall, both the simulated annealing and the linearized travel-time inversion results are superior to the straight-ray backprojection in reconstructing the velocity structure. The improvement is due to the inclusion of wave refraction effects in the inversions. The 20% velocity variations are too large for the straight ray approximation. However, even the straight ray result produces useful information on the structure. The linearized inversion scheme has the advantage in this test of containing the ideal parameterization to match the target model. The major problem with the annealing results appears to be the effects resulting from the velocity perturbation scheme used in the search. Larger artifacts would be expected in tomographic problems with a less ideal source-receiver distribution.

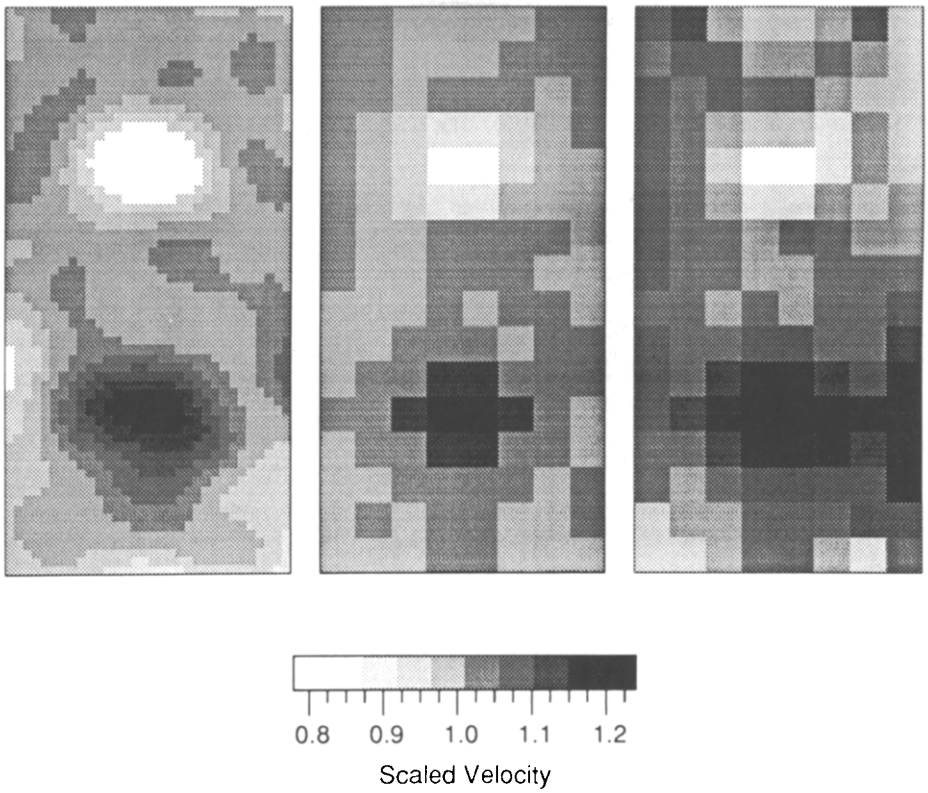

FIG. 10. A comparison of "Cross Model" inversions. The simulated annealing inversion result is on the *left*, the linearized traveltime inversion is in the *center*, and a straight-ray backprojection result is on the *right*. The observations used in these inversions are without noise.

SURFACE-WAVE INVERSION

As a final illustration of the linearized inversion technique, we have inverted a subset of the Rayleigh-wave phase-velocity measurements used in the surface-wave regionalization study of the western United States performed by Taylor and Patton (1986). Our purpose here is to present an example of the inversion scheme applied to actual seismic data, not a detailed analysis of these data or the resulting model. Only preliminary results are shown since further study of the western United States is planned using an expanded phase-velocity data set. Figure 11 presents the great-circle paths connecting the source-receiver pairs used in the inversion. As seen from Figure 11, the region of best coverage is in the central and northern Basin and Range province of the western United States. A least-squares fit of a constant phase velocity model to 66 phase travel times measured at 10-sec-period produces a phase velocity estimate of 3.16 km/sec and an overall mean-square error of 19.2 sec^2. The 10-sec Rayleigh waves are most sensitive to the upper crustal depths. In Figure 12 we present the results of an inversion of the 10-sec period phase measurements. The model shown results from a three iteration inversion. The convergence of the inversion was rapid; most of the major features in the model are present after the first iteration. The mean square error for this model is 4.36 sec^2. Several interesting features are present in this reconstruction. Particu-

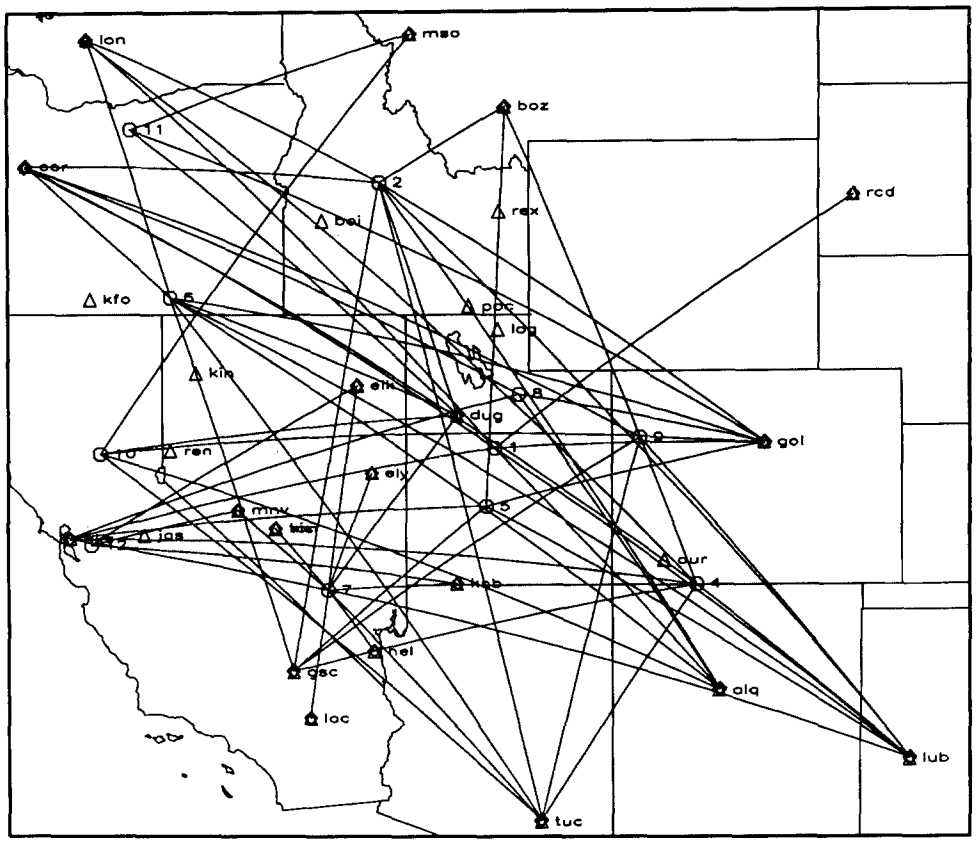

FIG. 11. Great-circle paths for the 10-sec-period Rayleigh-wave phase observations used in the travel-time inversion.

larly, the high velocities in the Idaho region and the ridge of relatively fast velocities beneath central Utah. These preliminary results agree with the original work of Taylor and Patton (1986) and also agree well with the recent modeling efforts of Yan (1990), who used a great-circle inversion for Fourier coefficients of the phase-velocity variation throughout the western United States.

DISCUSSION

The numerical tests demonstrate that the linearized travel-time inversion technique performs best on smooth models but is also successful on the rougher, constructed models typically used to test other travel-time inversion techniques. The influence of noise is minimal on the stability of the technique, and the ability to require smooth resulting models allows one to limit the effect of approximately random travel-time fluctuations. The convergence is quick and stable, and no divergence has been observed. The simulated annealing approach also performed well in the test inversion. Although the random perturbations scheme utilized here introduces minor artifacts into the model, averaging the results of several searches reduces the importance of these artifacts on the final slowness estimate. At present, because of its slightly better performance, computational speed, and the wealth of information and understanding on linearized least-squares approaches, the linearized inversion is the preferable

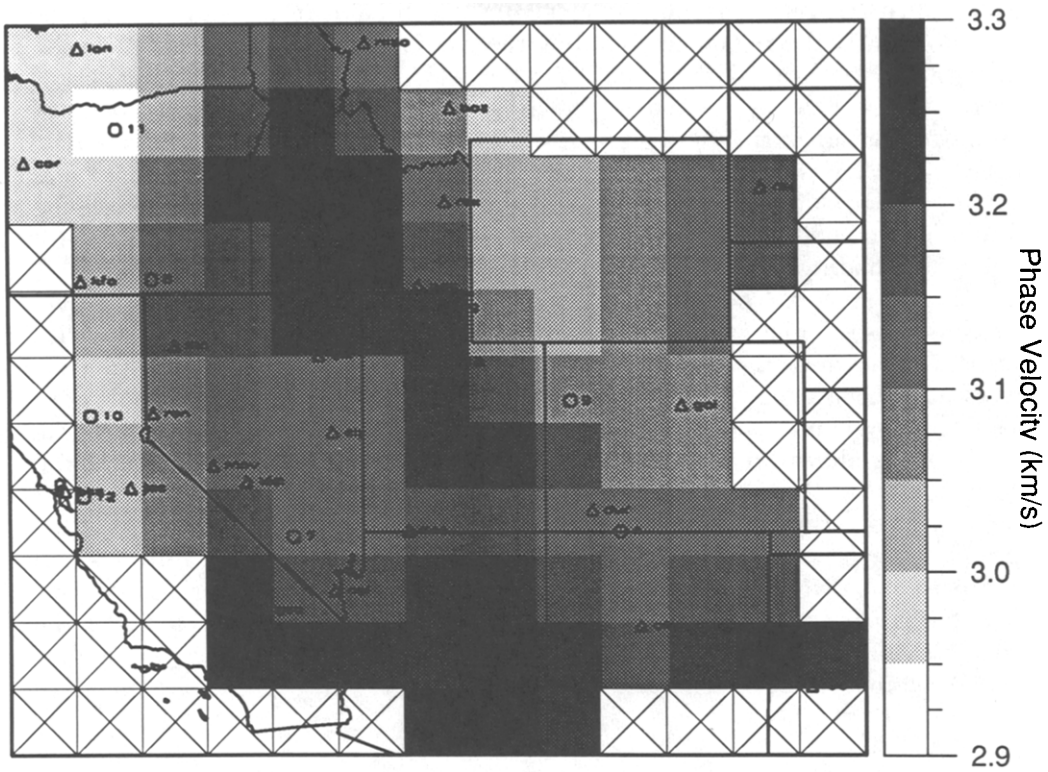

FIG. 12. Inversion results after three iterations of the Rayleigh-wave phase measurements. Cells marked with an X were held constant during the inversion. Stations are identified by triangles and sources are identified by circles.

technique. Implementation of the annealing algorithm on parallel processors will make that scheme more promising. Also, when wave paths travel large distances in strongly heterogeneous media, the linearized approach may fail due to an inadequate starting model. Although we have not investigated these circumstances, we suspect that in these cases the nonlinear approach of simulated annealing may prove more effective.

The linearized inversion calculations presented above were performed on a Sun Sparc Station. Each iteration required approximately 10 minutes of computer time. The singular value decomposition of the partial derivative matrix expended about one half of the computation time. For larger-scale problems, faster methods (Nolet, 1987) for solving the algebraic system can be employed. The travel-time derivative calculations are the second largest computer expense during the inversion. Of course, these computation costs are problem dependent. For all the tests presented here, a travel-time derivative is calculated at each cell for each observation. Obviously it is inefficient to calculate the derivatives for each cell when we know a limited number of cells affect the travel time of a given wave. For example, the cells near the top of the model have no influence on the travel times between a source and receiver near the bottom of the model.

The finite-difference travel-time calculation scheme provides a simple approach to identifying those cells that influence a specific travel-time observation. If we sum the travel time from the source to each point in a travel-time

grid and the travel time from the receiver to each point in the slowness image, we can identify the region surrounding the wave's travel path. Roughly, we can map the "ray width" (Nolet, 1987) for the wave. The area of nonzero partial derivatives is directly related to the Fresnel zone and is of interest in itself. However, for our purposes we only desire to define the region of nonzero partial derivatives. The addition of source and receiver time images has been used in a similar way to calculate ray paths using the finite-difference travel-time scheme (Pullammanappallil *et al.*, 1991). A sample ray width is presented in Figure 13. The gray shading is used to contour the sum of the source and the receiver travel-time images. This sum has a minimum value equal to the wave travel time (43.1 sec). For comparison, the partial derivatives of travel time with respect to slowness for this observation are also displayed. The partial derivatives have been clipped at a maximum amplitude of 1.0 for plotting purposes. The true maximum partial derivative value is approximately 4.0; the true minimum is shown in the figure. For our purposes, we could calculate partial derivatives for those cells that contain travel times less than 45 sec. This conservative estimate would require partial derivatives for 33 cells. As illustrated by the extent of the ray sensitivity, the reliance on rays of infinitesimal width is not always a very good approximation for seismic observations. Our calculation of partial derivatives using a finite-difference approach includes the effects of ray-path changes, since we recalculate the travel times through a perturbed model to construct the derivative. However, our choice of a one-sided

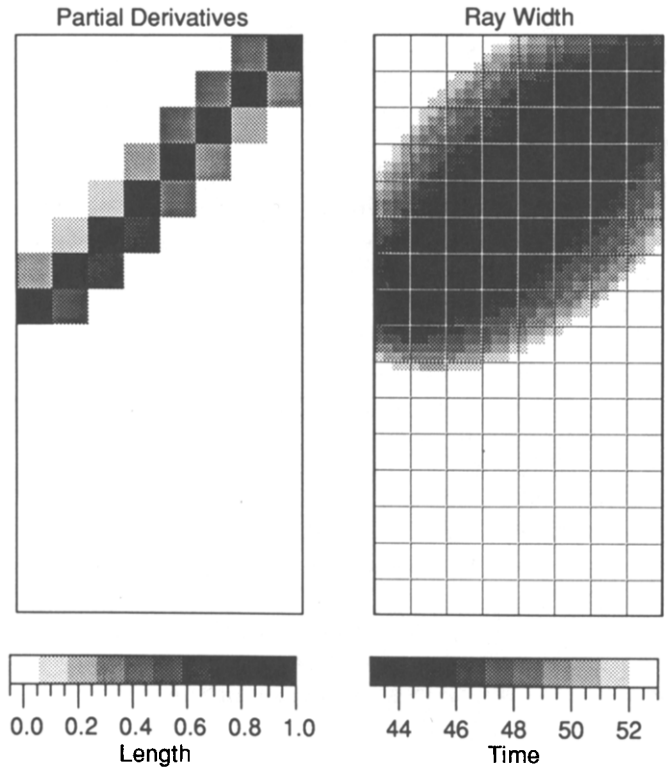

FIG. 13. Partial derivatives (*left*) and the ray width (*right*) calculated through the model shown to the left in Figure 7 (smooth model 1).

difference still limits our derivative accuracy to first-order in slowness. The result is that our region of sensitivity is somewhat wider than a typical ray path but still may be less than the Fresnel zone of band-limited data. Usually, allowance for errors in the ray width are made during the selection of the cell dimensions or a combination of cell dimension and smoothness constraints.

The total number of calculations needed to identify the ray width is one for the source and one for each receiver. The partial derivatives would then be calculated for each node in the region of ray sensitivity. For well-distributed receivers, many cells will require partial derivatives and the ray width calculation would not save much computing time. If, however, a source radiates to a group of receiver in a limited part of the model, the ray width calculations could result in significant time savings. The computational savings derived from the use of ray widths to define the area of ray sensitivity would be most dramatic in three-dimensional problems. We note also that the calculations necessary for the ray widths are identical to those necessary for an iterative inversion of local earthquake arrival times with a relocation of the events between iterations (using the location scheme of Nelson and Vidale (1990)).

Conclusion

We have presented a new method for inverting seismic travel times to estimate subsurface geologic structure. The technique is based on a linearized least-squares inversion of the travel-time residuals. The iterative procedure includes the effects of ray bending. Additionally, the inversion scheme allows smoothness constraints to be placed on the resulting solutions converges quickly, and is stable. A simulated annealing search also performs reasonably well in the travel-time inversion problem. The models resulting from these inversions may contain poorly constrained artifacts of the perturbation procedure and a careful analysis of the results is necessary prior to interpretation of the model, particularly in studies with inadequate ray coverage. Potential applications of eikonal-equation based inversions are numerous. Most obvious are the borehole transmission tomography and surface-wave phase velocity problems illustrated here. Other possibilities include the inversion of reflection data (Pullammanappallil *et al.*, 1991), refraction studies, and regional-scale mantle studies.

Acknowledgments

We would like to thank Chuck Langston, George Zandt, and John Louie for the help during this project. We thank Howard Patton for supplying the western United States phase velocity observations. Thanks go to Harley Benz, Bob Clouser, Satish Pullammanappallil, Robert Polzer, Roy Greenfield, Thorne Lay, and two reviewers for their comments on this research and on the manuscript. Much of this work was performed while C.J.A. was a graduate student at the Pennsylvania State University. Support for this work during this time was provided by the Penn State Geosciences Department Shell fellowship. The completion of this work at UCSC was supported by NSF Grant CEAR 8451715, the W. M. Keck Foundation, and the Southern California Earthquake Center under the authority of Cooperative Agreement Number 14-08-00001-A0899 issued by the U.S. Geological Survey. Contribution Number 132 of the Institute of Tectonics and C. F. Richter Seismological Laboratory of the University of California at Santa Cruz.

References

Aarts, E. and J. Korst (1989). *Simulated Annealing and Boltzmann Machines: A Stochastic Approach to Combinatorial Optimization and Neural Computing*, Wiley, Chichester.

Berryman, J. G. (1989a). Fermat's principle and nonlinear traveltime tomography, *Phys. Rev. Lett.*, **62**, 2953–2956.

Berryman, J. G. (1989b). Weighted least-squares criteria for seismic traveltime tomography, *IEEE Trans. Geosci. and Remote Sensing* **27**, 302–309.

Berryman, J. G. (1990). Lecture notes on nonlinear inversion and tomography, Lawrence Livermore National Laboratory Report, UCRL-LR-105358.

Bregman, N. D., R. C. Bailey, and C. H. Chapman (1989). Crosshole seismic tomography, *Geophysics* **54**, 200–215.

Constable, S. C., R. L. Parker, and C. G. Constable (1987). Occam's inversion: a practical algorithm for generating smooth models from electromagnetic sounding data, *Geophysics* **52**, 289–300.

Frazer, L. N. (1990). Geophysical inversion with simulated annealing and genetic algorithms, *Eos* **71**, 1477.

Jackson, D. D. (1972). Interpretation of inaccurate, insufficient, and inconsistent data, *Geophys. J. Royal Astr. Soc.* **28**, 97–109.

Kirkpatrick, S., C. D. Gelatt Jr., and M. P. Vecchi (1983). Optimization by simulated annealing, *Science* **220**, 671–680.

Landa, E., W. Beydoun, and A. Tarantola (1989). Reference velocity model estimation from prestack waveforms: coherency optimization by simulated annealing, *Geophysics* **54**, 984–990.

Lees, J. M. and R. S. Crosson (1989). Tomographic inversion for three-dimensional velocity structure at Mount St. Helens using earthquake data, *J. Geophys. Res.*, **94**, 5716–5728.

Metropolis, N., N. Rosenbluth, M. Rosenbluth, A. Teller, and E. Teller (1953). Equations of state calculations by fast computing machines, *J. Chemical Phys.* **21**, 1087–1092.

Nelson, G. D. and J. E. Vidale (1990). Earthquake locations by 3-D finite-difference travel times, *Bull. Seism. Soc. Am.* **80**, 395–410.

Nolet, G. (1987). *Seismic Tomography*, Reidel, Dordrecht, Holland.

Press, W. H., B. P. Flannery, S. A. Teukolsky, and W. T. Vetterling (1988). *Numerical Recipes in C*, Cambridge University Press, New York.

Pullammanappallil, S., C. J. Ammon, and J. N. Louie (1991). Inversion of reflection times without raytracing, *Seism. Res. Lett.* **62**, 19.

Rothman, D. H. (1985). Nonlinear inversion, statistical mechanics, and residual statics estimation, *Geophysics* **50**, 2797–2807.

Rothman, D. H. (1986). Automatic estimation of large residual statics corrections, *Geophysics* **51**, 332–346.

Shaw, P. R. and J. A. Orcutt (1985). Waveform inversion of seismic refraction data and applications to young Pacific crust, *Geophys. J. R. Astr. Soc.* **82**, 375–415.

Trantola, A. (1987). *Inverse Problem Theory: Methods for Data Fitting and Model Parameter Estimation*, Elsevier, Amsterdam.

Taylor, S. R. and H. J. Patton (1986). Shear-velocity from regionalized surface-wave dispersion in the Basin and Range, *Geophys. Res. Lett.* **31**, 30–33.

Vidale, J. E. (1988). Finite-difference calculation of travel times, *Bull. Seism. Soc. Am.* **78**, 2062–2076.

Vidale, J. E. (1991). Finite-difference calculations of traveltimes in three dimensions, *Geophysics* **55**, 521–526.

Vidale, J. E. (1993). Accurate finite-difference traveltimes amidst severe velocity contrasts (manuscript in preparation).

Wiggins, R. (1972). The general linear inverse problem: implication of surface waves and free oscillations on Earth structure, *Rev. Geophys. Space Phys.* **10**, 251–285.

Yan, B. (1990). Inversion of surface-wave slowness data for crustal structure using 2-D Fourier coefficient method, *Ph.D. Thesis*, The Pennsylvania State University, University Park, PA.

INSTITUTE OF TECTONICS
UNIVERSITY OF CALIFORNIA AT SANTA CRUZ
SANTA CRUZ, CALIFORNIA 95064
(C. J. A.)

JOHN E. VIDALE
U.S. GEOLOGICAL SURVEY
345 MIDDLEFIELD ROAD
MENLO PARK, CALIFORNIA 94025
(J. E. V.)

Manuscript received 6 June 1991